Structural Analysis of Altered Large-Subunit Loop-6/Carboxy-Terminus Interactions That Influence Catalytic Efficiency and CO_2/O_2 Specificity of Ribulose-1,5-bisphosphate Carboxylase/Oxygenase[†,‡]

Saeid Karkehabadi,[§] Sriram Satagopan,[||,⊥] Thomas C. Taylor,[§] Robert J. Spreitzer,[||] and Inger Andersson*[,§]

Department of Molecular Biology, Swedish University of Agricultural Sciences, BMC Box 590, 751 24 Uppsala, Sweden, and Department of Biochemistry, University of Nebraska, Lincoln, Nebraska 68588

Received May 31, 2007; Revised Manuscript Received July 23, 2007

ABSTRACT: The loop between α-helix 6 and *β*-strand 6 in the α/*β*-barrel of ribulose-1,5-bisphosphate carboxylase/oxygenase plays a key role in discriminating between CO_2 and O_2. Genetic screening in *Chlamydomonas reinhardtii* previously identified a loop-6 V331A substitution that decreases carboxylation and CO_2/O_2 specificity. Revertant selection identified T342I and G344S substitutions that restore photosynthetic growth by increasing carboxylation and specificity of the V331A enzyme. In numerous X-ray crystal structures, loop 6 is closed or open depending on the activation state of the enzyme and the presence or absence of ligands. The carboxy terminus folds over loop 6 in the closed state. To study the molecular basis for catalysis, directed mutagenesis and chloroplast transformation were used to create T342I and G344S substitutions alone. X-ray crystal structures were then solved for the V331A, V331A/T342I, T342I, and V331A/G344S enzymes, as well as for a D473E enzyme created to assess the role of the carboxy terminus in loop-6 closure. V331A disturbs a hydrophobic pocket, abolishing several van der Waals interactions. These changes are complemented by T342I and G344S, both of which alone cause decreases in CO_2/O_2 specificity. In the V331A/T342I revertant enzyme, Arg339 main-chain atoms are displaced. In V331A/G344S, α-helix 6 is shifted. D473E causes disorder of the carboxy terminus, but loop 6 remains closed. Interactions between a transition-state analogue and several residues are altered in the mutant enzymes. However, active-site Lys334 at the apex of loop 6 has a normal conformation. A variety of subtle interactions must be responsible for catalytic efficiency and CO_2/O_2 specificity.

Ribulose-1,5-bisphosphate carboxylase/oxygenase (Rubisco,[1] EC 4.1.1.39) serves as the key enzyme for photosynthetic carbon assimilation by catalyzing the rate-limiting reaction of CO_2 with ribulose 1,5-bisphosphate (RuBP) to form two molecules of 3-phosphoglycerate (reviewed in refs *1*−*3*). Rubisco also catalyzes an oxygenase reaction in which O_2 competes with CO_2 for the same enediol intermediate of RuBP. Competitive oxygenation of RuBP generates one molecule of 3-phosphoglycerate and one molecule of 2-phosphoglycolate. The latter product initiates photorespiration, a seemingly futile pathway that causes a considerable decrease in the rate of photosynthetic biomass assimilation. Coupled with its slow turnover, activity regulation by a chaperone-like Rubisco activase protein, and complex quaternary structure, there has been much interest in engineering an improved Rubisco enzyme as a means for increasing agricultural productivity (reviewed in refs *1*−*6*).

The Rubisco CO_2/O_2 specificity factor (Ω) is defined as the ratio of the catalytic efficiencies of carboxylation (V_c/K_c) and oxygenation (V_o/K_o), where V is the V_{max} of either carboxylation or oxygenation and K is the Michaelis constant for CO_2 or O_2 (*7*), and is proportional to the difference in free energies of activation for the carboxylation and oxygenation transition states (*8*). There is considerable variation in Ω among Rubisco enzymes from different species (*9*−*11*). Structural differences relatively far from the active site may contribute to this variation (*12*−*14*).

Rubisco from most prokaryotes and all eukaryotes is a hexadecamer (reviewed in ref *2*). In land plants and green algae, two ∼55 kDa large subunits (encoded by the chloroplast *rbcL* gene) assemble into functional dimers with two active sites at the interface. A core comprised of four of these dimers is capped at each end by four ∼15 kDa small subunits (encoded by a family of *rbcS* nuclear genes). X-ray crystal structures of Rubisco enzymes from prokaryotes, algae, and

[†] This work was supported by the Swedish Research Council for Environment, Agricultural Sciences, and Spatial Planning (FORMAS), the European Union (Grant No. QLK3-CT-2002-01945), and the U.S. Department of Agriculture National Research Initiative (Grant No. 2006-35318-17376).

[‡] Coordinates and structure factors for the mutant enzymes have been deposited in the Protein Data Bank with accession codes 2v63 for V331A, 2v67 for T342I, 2v68 for V331A/T342I, 2v6a for V331A/G344S, and 2v69 for D473E.

* To whom correspondence should be addressed. Phone: +46-18-4714288. Fax: +46-18-536971. E-mail: inger@xray.bmc.uu.se.

[§] Swedish University of Agricultural University.

[||] University of Nebraska.

[⊥] Current address: Department of Microbiology, Ohio State University, Columbus, OH 43210.

[1] Abbreviations: Rubisco, D-ribulose-1,5-bisphosphate carboxylase/oxygenase; RuBP, D-ribulose 1,5-bisphosphate; Ω, CO_2/O_2 specificity factor; V_c, V_{max} for carboxylation; V_o, V_{max} for oxygenation; K_c, Michaelis constant for CO_2; K_o, Michaelis constant for O_2; PDB, Protein Data Bank; CABP, 2-carboxyarabinitol 1,5-bisphosphate; NCS, noncrystallographic symmetry.

10.1021/bi701063f CCC: $37.00
Published on Web 09/08/2007

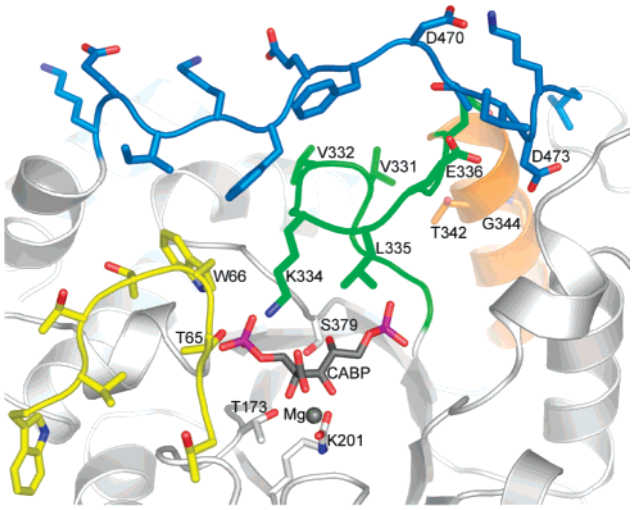

FIGURE 1: Loop 6 and associated structural regions in the X-ray crystal structure of *Chlamydomonas* Rubisco (PDB 1GK8) (*29*). Loop 6 (residues 328−338) is colored green, α-helix 6 (residues 339−350) is colored orange, the carboxy-terminal strand (residues 463−475) is colored blue. and an amino-terminal loop (residues 63−70) of a neighboring large subunit is colored yellow.

land plants reveal a striking similarity among the large subunits.

The large subunit contains a carboxy-terminal α/*β*-barrel that forms a rigid framework for the active site. Loops of the α/*β*-barrel domain of one subunit and residues in the amino-terminal domain of the other subunit in the dimer contribute invariant residues that interact with the substrate (*15*). Whereas the majority of these loops form part of the rigid framework of the active site, some loops are flexible and move during catalysis. Judging from the available structures in the Protein Data Bank (PDB), the movements are strict, and partition Rubisco structures into two states, either open or closed (*16*). The open state is associated with an unliganded active site or an active site occupied by loosely bound ligands (substrates or products). The closed state, in contrast, is associated with tightly bound substrates or inhibitors. A closed active site is completely shielded from solvent and able to sustain catalysis (*16*).

The transition between open and closed active sites is well-defined (*17*, *18*). When the active site closes, there is a rigid-body movement that brings the amino- and carboxy-terminal domains of adjacent subunits together, residues 63−69 of the amino-terminal domain become ordered, part of the loop between *β*-strand 6 and α-helix 6 of the α/*β*-barrel (residues 331−338 of loop 6) closes over the active site, and the carboxy-terminal strand (residues Trp463 to the end) packs against loop 6 (Figure 1). Thus, loop 6 plays a critical role in both carboxylation and oxygenation.

The sequence of loop 6 is well-conserved among land plants and green algae. Apart from Gly333 and Gly337, which are likely conserved to maintain flexibility in the hinge of the loop, one residue, Lys334, is strictly conserved (Figure 1). Crystallographic analysis of activated Rubisco complexed with the transition-state analogue 2-carboxyarabinitol 1,5-bisphosphate (CABP) reveals the importance of Lys334 in orienting and stabilizing the intermediate (*19*). The side chain of Lys334, which is situated at the tip of loop 6, extends into the active site and hydrogen bonds to the two oxygen atoms of CABP that are equivalent to those of substrate CO_2. It also makes hydrogen bonds with the *γ*-carboxylate of Glu60 and the hydroxyl group of Thr65 in the amino-terminal domain of the adjacent large subunit. Directed mutagenesis studies of Rubisco from *Rhodospirillum rubrum* and *Synechococcus* demonstrated that alterations at Lys334 can cause dramatic decreases in carboxylation and Ω (*20*−*23*).

The transition of loop 6 from the open to closed form involves changes in the *ϕ* and *ψ* torsion angles of residues Val332 and Glu338 (*16*). The adjacent Gly333 and Gly337 provide the flexibility required for the transition. Another residue, Val331, also appears to form part of the hinge on which loop 6 moves (Figure 1). This residue is also highly, but not strictly, conserved (*24*).

The importance of loop 6 and Val331 was originally demonstrated by genetic screening in the green alga *Chlamydomonas reinhardtii* (*25*). Replacement of Val331 by Ala caused considerable reduction in Ω and carboxylation catalytic efficiency. Genetic selection for restored photosynthesis identified T342I and G344S substitutions that increased Ω with only a modest improvement in V_c/K_c (*25*, *26*). The fact that residues 331, 342, and 344 flank the strictly conserved Lys334 situated at the tip of loop 6 stressed the importance of this loop for catalysis and specificity in Rubisco (Figure 1). Despite conflicting results between two subsequent studies, directed mutagenesis generally confirmed the importance of residues 331 and 342 in *Synechococcus* Rubisco (*22*, *27*).

Apart from the transition observed in loop 6, movement of the carboxy terminus against loop 6 also seems to be intimately involved in the transition from the open to the closed state of the Rubisco active site (*17*, *18*). In particular, Asp473 was proposed to serve as a latch responsible for placing the large-subunit carboxy terminus over loop 6, thereby stabilizing the closed conformation required for catalysis (*16*) (Figure 1). However, directed mutagenesis and chloroplast transformation in *Chlamydomonas* showed that Asp473 is not essential for catalysis. D473A and D473E mutant enzymes supported near-wild-type photosynthetic growth despite substantial decreases in Ω and V_c/K_c (*28*).

To better understand the structural role of loop 6 and the carboxy terminus in Rubisco catalysis, suppressor-mutant enzymes T342I and G344S were created by directed mutagenesis and chloroplast transformation of *Chlamydomonas*. The kinetic properties of the purified mutant enzymes were determined. X-ray crystal structures were solved for the original *Chlamydomonas* V331A-mutant enzyme, V331A/T342I- and V331A/G344S-revertant enzymes, and T342I-suppressor enzyme. A lower resolution (2.8 Å) crystal structure was also obtained for the carboxy-terminal D473E-mutant enzyme. These structures were compared to each other and to the 1.4 Å structure of wild-type *Chlamydomonas* Rubisco (*29*).

MATERIALS AND METHODS

Strains and Culture Conditions. C. reinhardtii 2137 mt^+ is the wild-type strain (*30*). The *rbcL*-V331A mutant was recovered previously by genetic screening for an acetate-requiring phenotype (*8*). Photosynthesis-competent *rbcL* revertants V331A/T342I and V331A/G344S, which arose from intragenic suppression, were recovered by genetic selection on minimal medium in light (*8*, *26*). Mutant strain

MX3312 mt^+ is used as the host for chloroplast transformation (*28*). It lacks photosynthesis and requires acetate for growth due to the engineered replacement of *rbcL* with the bacterial *aadA* gene (*31*). The *rbcL*-D473E mutant was created previously by directed mutagenesis, chloroplast transformation of MX3312, and selection for photosynthetic growth (*28*). All *Chlamydomonas* strains were maintained at 25 °C in darkness with 10 mM acetate medium containing 1.5% Bacto agar (*30*). For routine biochemical analysis, cells were grown on a rotary shaker at 220 rpm with 250−500 mL of liquid acetate medium in darkness.

Directed Mutagenesis and Chloroplast Transformation. Using a plasmid containing the *Chlamydomonas rbcL* gene (*32*), directed mutagenesis was performed using synthetic oligonucleotides and a QuickChange mutagenesis kit from Stratagene (*33*). To create the T342I substitution, the sequence ACT was changed to ATT. The G344S substitution was created by changing GGT to TCT, which eliminated a recognition site for *Bfa*I as an aid for subsequent screening. Following amplification in *Escherichia coli* XL1-Blue (Stratagene), the resultant mutant plasmids, named pLS-T342I and pLS-G344S, were transformed into the chloroplast of *rbcL*-mutant MX3312 by using a helium-driven biolistic device (*34*). Photosynthesis-competent transformants were selected on minimal medium in light (80 μmol of photons m^{-2} s^{-1}) by standard methods (*28*, *32*). Successive rounds of selection, single-colony isolation, and restriction-enzyme analysis were performed to ensure the homoplasmicity of the mutant genes (*28*, *32*). The mutant *rbcL* genes were PCR amplified and completely sequenced at the DNA sequencing facility of the University of Nebraska (Lincoln, NE) to confirm that only the intended mutations were present. The mutant *Chlamydomonas* strains were named T342I and G344S.

Biochemical Analysis. Rubisco holoenzyme was purified from dark-grown cells on sucrose gradients containing 50 mM *N*,*N*-bis(2-hydroxyethyl)glycine (pH 8.0), 10 mM $NaHCO_3$, 10 mM $MgCl_2$, and 1 mM dithiothreitol (*35*). The carboxylation and oxygenation kinetic constants of purified and activated enzymes were assayed in the same buffer by measuring the incorporation of acid-stable ^{14}C from $NaH^{14}CO_3$ (*36*). Ω was determined with 20 μg of Rubisco per reaction by assaying carboxylase and oxygenase activities simultaneously with 44 μM [1-^{3}H]RuBP (15.8 Ci/mol) and 2 mM $NaH^{14}CO_3$ (5.0 Ci/mol) in 30 min reactions at 25 °C (*37*, *38*). The phosphoglycolate phosphatase and [1-^{3}H]RuBP used in the assays were synthesized/purified according to standard methods (*37*, *39*).

Purification, Crystallization, and Data Collection. To obtain large quantities of Rubisco for structural analysis, 3−5 L of cell culture were concentrated by centrifugation, and the cells were lysed by sonication. Protein was precipitated with ammonium sulfate between 30% and 50% saturation. The redissolved cellular material was loaded onto a Superdex-200 Hiload 16/60 size exclusion column (GE Healthcare Life Sciences), and fractions corresponding to Rubisco were collected and loaded onto a MonoQ anion exchange column. Rubisco was eluted from the column with a 0.1−0.5 M NaCl gradient. Purified protein was concentrated to 10 mg/mL in an activating buffer containing 50 mM HEPES (pH 7.5), 10 mM $NaHCO_3$, and 5 mM $MgCl_2$. Crystals of the mutant Rubisco enzymes were grown using the hanging-drop vapor diffusion method at 20 °C. The drops were prepared by mixing a protein solution containing 10 mg/mL Rubisco and 1 mM CABP with an equal amount of a well solution containing 50 mM HEPES (pH 7.5), 0.05−0.2 M NaCl, 7−12% poly(ethylene glycol) 4000, 10 mM $NaHCO_3$, and 5 mM $MgCl_2$. Crystals grew within 1 week. Prior to data collection, crystals were frozen in liquid N_2 using a mother liquor with 30% ethylene glycol added as a cryoprotectant. Data for the V331A/T342I and D473E mutant enzymes were collected on beamline I711 at Max-lab, Lund, Sweden. Data for the V331A and T342I enzymes were collected on beamline ID14-1 and those for the V331A/G344S enzyme on beamline ID14-3 at the European Synchrotron Radiation Facility, Grenoble, France. A single crystal was used in each case. The data were processed using DENZO and SCALEPACK (*40*).

Structure Determination and Refinement. The mutant crystal structures were solved by molecular replacement using the program MOLREP (*41*, *42*). The search object consisted of half a molecule of wild-type *Chlamydomonas* Rubisco (four large and four small subunits), PDB code 1GK8 (*39*), in which the mutated residues were deleted. Refinement was performed using REFMAC5 (*43*). For cross-validation, 5% of the data were excluded from the refinement for R_{free} calculations. Initial $2F_o - F_c$ and $F_o - F_c$ electron density maps, calculated after one round of rigid body refinement of individual large and small subunits using data between 20 and 3 Å, showed clear density for the mutated residues except in the case of D473E, in which the substitution causes disorder of residues 470−475. After the substituted residues were built into the density, the mutant structures were further refined using a maximum likelihood target function and overall *B*-factor refinement. Tight non-crystallographic symmetry (NCS) restraints were imposed at the beginning of the refinement for all structures. Toward the end of refinement, NCS restraints were relaxed or removed for regions of the structure that clearly deviated from NCS. Analysis of the structures revealed that the majority of the deviations are caused by close-packing interactions in the crystal. In the structures of the V331A, T342S, and V331A/T342S enzymes, close contacts involve residues 439 of the large subunit and residues 84 and 130−140 of the small subunit. NCS restraints were thus removed entirely from these residues. The V331A/G344S enzyme crystallizes in a different space group ($P2_12_12_1$ instead of $P2_1$). In this case, loop 91−95 of the large subunit deviates from NCS in two of the subunits (A and E) and was thus excluded from NCS restraints. In addition, the high resolution of this structure (1.5 Å) permitted a slight relaxation of restraints on amino acid side chains toward the end of the refinement. The structure of the D473E enzyme is of low resolution (2.8 Å). Therefore, tight NCS restraints were maintained throughout refinement in this case. Solvent molecules were added using ARP/wARP (*44*). Throughout the refinement, $2mF_o - DF_c$ and $mF_o - DF_c$ sigmaA-weighted maps (*45*) were inspected and the models manually adjusted in O (*46*).

RESULTS

Recovery and Analysis of Mutant Enzymes. As a means for further elucidating the contribution of loop-6 residues to the function of Rubisco, suppressor substitutions were created in the absence of the original V331A-mutant substitution.

Table 1: Kinetic Properties of Rubisco Purified from the Wild Type, Mutant V331A, Revertants V331A/T342I and V331A/G344S, and Suppressor Mutants T342I and G344S

enzyme	Ω^a (V_cK_o/V_oK_c)	$V_c{}^a$ (μmol h^{-1} mg^{-1})	$K_c{}^a$ (μM CO_2)	$K_o{}^a$ (μM O_2)	$V_c/K_c{}^b$	$K_o/K_c{}^b$	$V_c/V_o{}^b$
wild type	63 ± 1	116 ± 8	36 ± 1	448 ± 74	3.2	12	5.3
V331A	25 ± 4	4 ± 1	162 ± 17	1921 ± 254	<0.1	12	2.1
V331A/T342I	51 ± 2	39 ± 12	54 ± 5	758 ± 102	0.7	14	3.6
V331A/G344S	44 ± 3	25 ± 5	91 ± 8	933 ± 99	0.3	10	4.4
T342I	54 ± 2	56 ± 19	42 ± 5	700 ± 169	1.3	17	3.2
G344S	57 ± 2	63 ± 13	26 ± 3	217 ± 34	2.4	8	7.1

[a] Values are the means ± standard deviation ($n - 1$) of three separate enzyme preparations. [b] Calculated values.

Table 2: Statistics for Data Collection and Refinement

	V331A	V331A/T342I	T342I	V331A/ G344S	D473E
resolution limit[a] (Å)	1.8 (1.83−1.80)[d]	2.3 (2.29−2.25)	2.0 (2.03−2.00)	1.5 (1.54−1.50)	2.8 (2.90−2.80)
space group	$P2_1$	$P2_1$	$P2_1$	$P2_12_12_1$	$P2_1$
cell dimensions					
a, *b*, *c* (Å)	121.4, 177.4, 122.6	120.4, 178.2, 122.6	120.1, 178.6, 122.5	129.9, 196.6, 202.0	114.2, 169.1, 137.2
β (deg)	117.6	117.7	117.8	90.0	96.2
no. of reflns					
measured	1 359 564	1 285 694	708 970	3 301 610	342 049
unique	389 935	221 744	272 649	781 039	125 065
completeness (%)	92.4 (60.0)	99.2 (88.6)	89.2 (89.9)	96.0 (89.9)	98.4 (98.6)
I/σ	16.5 (2.4)	10.8 (3.1)	7.5 (1.3)	20.0 (1.9)	11.9 (1.8)
$R_{merge}{}^b$	0.232 (0.462)	0.156 (0.396)	0.126 (0.689)	0.083 (0.525)	0.094 (0.626)
mean *B*-factor $B_W{}^a$ (Å^2)	15.04	19.39	17.96	19.24	59.61
$R_{cryst}{}^c$	0.191 (0.244)	0.171 (0.199)	0.174 (0.241)	0.176 (0.256)	0.197 (0.324)
$R_{free}{}^c$	0.214 (0.271)	0.202 (0.256)	0.207 (0.283)	0.192 (0.270)	0.228 (0.354)
estimated coordinate error[a] (Å)	0.088	0.142	0.112	0.046	0.298
rmsd from ideal geometry					
bond lengths (Å)	0.009	0.012	0.010	0.011	0.014
bond angles (deg)	1.16	1.28	1.19	1.29	1.40

[a] For the wild-type *Chlamydomonas* Rubisco structure (PDB code 1GK8), the resolution limit is 1.4 Å, the Wilson *B*-factor is 11.8 Å^2, and the estimated coordinate error (based on maximum likelihood calculations) is 0.034 Å. [b] $R_{merge} = \sum_h\sum_i|I_i(h) - \langle I_i(h)\rangle|/\sum_h\sum_i I_i(h)$, where $I(h)$ is the observed intensity and $\langle I(h)\rangle$ is the mean intensity of reflection *h*. [c] $R = \sum_{hkl}||F_o| - |F_c||/\sum_{hkl}|F_o|$, where F_o and F_c are the observed and calculated structure factor amplitudes, respectively. [d] Values in parentheses are for the highest resolution shell.

The *Chlamydomonas* T342I- and G344S-suppressor strains were recovered at wild-type *rbcL* transformation frequencies, displayed wild-type growth phenotypes, and had normal levels of Rubisco holoenzymes as measured via sucrose-gradient fractionation (data not shown). Thus, whereas both of the suppressor substitutions can restore photosynthetic growth of the original V331A mutant by increasing the Rubisco carboxylation rate and specificity (*8*, *36*), neither has any obvious effect on cell growth or Rubisco accumulation in the absence of the V331A substitution.

To determine whether the suppressor substitutions might increase the carboxylation rate or specificity of otherwise wild-type Rubisco, detailed kinetic analysis of the purified T342I- and G344S-suppressor enzymes was performed. As shown in Table 1 and previously (*8*, *36*), the T342I and G344S suppressor substitutions affect the kinetic properties of the original V331A-mutant enzyme in similar ways. Relative to the V331A enzyme, the V331A/T342I- and V331A/G344S-revertant enzymes have increases in Ω due to beneficial increases in V_c and decreases in K_c, and these increases in Ω occur despite ~2-fold decreases in K_o for both of the revertant enzymes. When the kinetic properties of the T342I- and G344S-suppressor enzymes (which contain wild-type Val-331) were determined (Table 1), both were found to have detrimental alterations in Rubisco catalytic properties. However, the suppressor substitutions affect catalysis in different ways. Relative to wild-type Rubisco, the V331A/T342I-revertant and T342I-suppressor enzymes have similar decreases in Ω and V_c, and increases in K_c and K_o (Table 1). Thus, the T342I substitution appears to be epistatic to the V331A substitution. In other words, T342I may alter the Rubisco structure in such a way as to make the effect of the identity of residue 331 (Val or Ala) insignificant. In contrast, the catalytic properties of the V331A/G344S-revertant enzyme appear to be intermediate (nonadditive) to those of the V331A-mutant and G344S-suppressor enzymes (Table 1). This may indicate that residues 331 and 344 interact with each other or a common structural or functional element that determines Rubisco catalytic efficiency and specificity. Despite a beneficial decrease in K_c, the G344S-suppressor enzyme has detrimental decreases in Ω, V_c, and K_o relative to the catalytic properties of the wild-type enzyme.

X-ray Crystal Structures of the Mutant Enzymes. To better understand the structural alterations and interactions brought about by residue substitutions in the loop-6 region, it was possible to solve the X-ray crystal structures of five of the mutant enzymes. The crystallographic data collection and refinement statistics for these crystal structures are summarized in Table 2. The quality of the structures is evidenced by the low values for R_{cryst} and R_{free} and the small deviations from ideal geometry. Clear density was observed for the substituted residues (Figure 2), and all enzymes showed density for all 140 residues of the small subunit. The amino-terminal residues of the large subunit were disordered in all structures, but the extent of disorder varied from subunit to

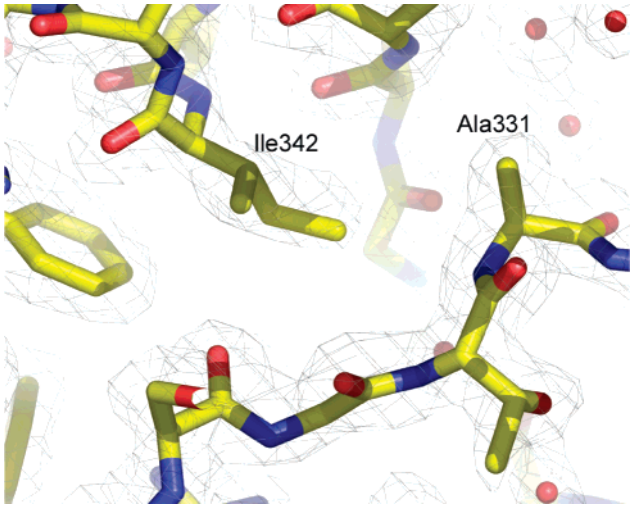

FIGURE 2: Electron density around the substituted residues in the V331A/T342I-revertant enzyme. The density is contoured at 1.0 σ, where σ represents the root-mean-square deviation from the mean density.

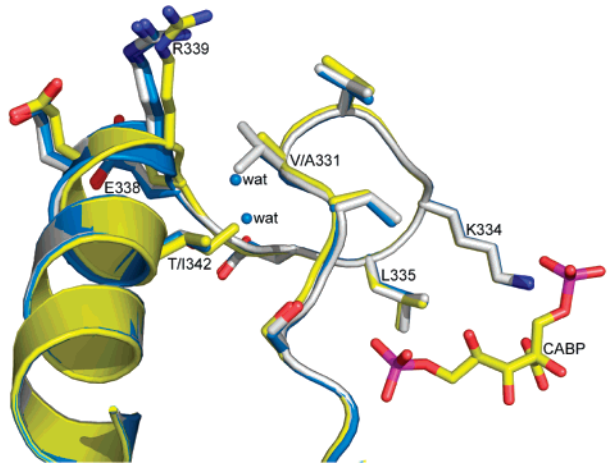

FIGURE 3: Outline of loop 6 in Rubisco from the *Chlamydomonas* wild type (carbon atoms colored white), mutant V331A (carbon atoms colored blue), and revertant V331A/T342I (carbon atoms colored yellow). Water molecules (wat, colored blue) are from the V331A-mutant enzyme structure (A-subunit only).

subunit. With some exceptions (see below), density was observed for residues 11−475 (from a total of 475 residues). However, in several of the subunits, an additional 2−4 amino-terminal residues could be built into the density. In the V331A-mutant enzyme, the last residue of the large subunit (475) was disordered. In the D473E-mutant enzyme, density was observed for large-subunit residues 11−469 except in one subunit (D), in which residues 470−474 could also be modeled. However, instead of folding over the active site, these residues point outward and are stabilized by the interaction with a neighboring molecule in the crystal. Thus, the relatively modest substitution of Asp473 by Glu causes disorder of the last six carboxy-terminal residues.

With the exception of local, but significant deviations close to the substituted residues in some of the mutant enzymes, no substantial shifts in large-subunit Cα backbone atoms are observed between the wild-type and mutant structures (Figure 3). A superposition of the individual wild-type large subunits with the large subunits of V331A, T342I, V331A/T342I, V331A/G344S, and D473E using the algorithms encoded in O (*46*) gave root-mean-square deviations of 0.20, 0.18, 0.25, 0.30, and 0.23 Å for all Cα atoms, respectively. These numbers are mean values for all eight subunits of the model. Although the values are close to the atomic coordinate error, it is interesting to note that the double-mutant revertant enzymes display greater deviation than that of the loop-6 single-mutant enzymes. The corresponding differences for the small subunit (residues 1−126) are 0.23, 0.21, 0.19, 0.21, and 0.34 Å, respectively. In the V331A/G344S-revertant enzyme, the substitution of Gly344 by Ser causes a substantial displacement of almost the entire large-subunit α-helix 6 (residues 338−347, Figure 4), as well as residues 356−362 of an adjacent loop, causing a shift in backbone coordinates for these residues of approximately 1 Å. A large shift is also observed for residues 88−95 in a loop near the large-subunit amino terminus of the V331A/G344S-revertant enzyme. However, in this case the shift is only observed in two of the eight subunits of the structure and is most likely caused by crystal packing interactions. This loop may interact with Rubisco activase (*47*, *48*).

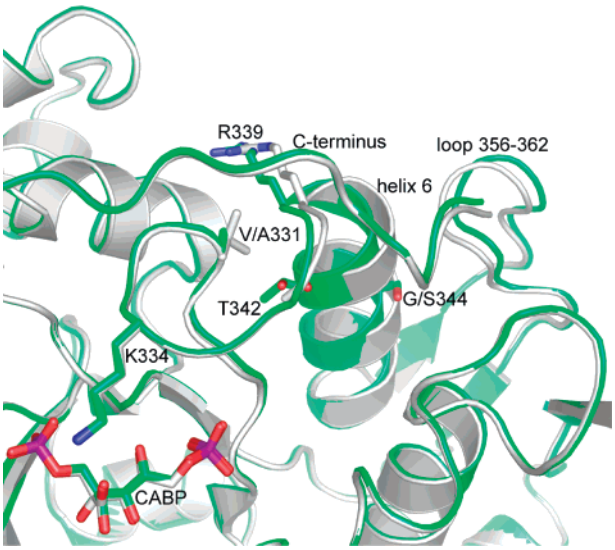

FIGURE 4: Shift of α-helix 6 and loop 356−362 in the V331A/G344S-revertant enzyme. Superposition of wild-type (white) and V331A/G344S-revertant (green) enzyme structures.

Perturbations in the Loop-6 Hydrophobic Core. The side chain of Val331 is situated in a hydrophobic pocket and has van der Waals interactions with residues Thr342 and Ile393 and the main-chain Cα atom of Arg339 (Figure 5A, Table 3). Substitution of the Val side chain by Ala in the V331A-mutant enzyme weakens these interactions considerably. In particular, the Ala Cβ atom does not make van der Waals contact with Thr342 (Figure 5A, Table 3). In at least one of the subunits, weak density was observed in the resultant cavity that most likely corresponds to two water molecules at low occupancy (Figure 3). In the V331A/T342I-revertant enzyme, van der Waals contact is restored between residues 331 and 342 (Figure 5B, Table 3). Most remarkable is the movement required to bring the Cα atom of residue Arg339 within van der Waals interaction distance with Ala331. This causes considerable displacement of the main-chain backbone of residues 337−343, with the Cα atom of Arg339 shifted by 0.87 Å (Figure 5B, Table 3). In principle a similar movement would be possible in the V331A-mutant enzyme, but no such shift was observed (Figure 5A). The presence of the additional Ile342 Cγ atom may be required to stabilize this shift. The additional bulk of the Ile342 Cγ atom in the

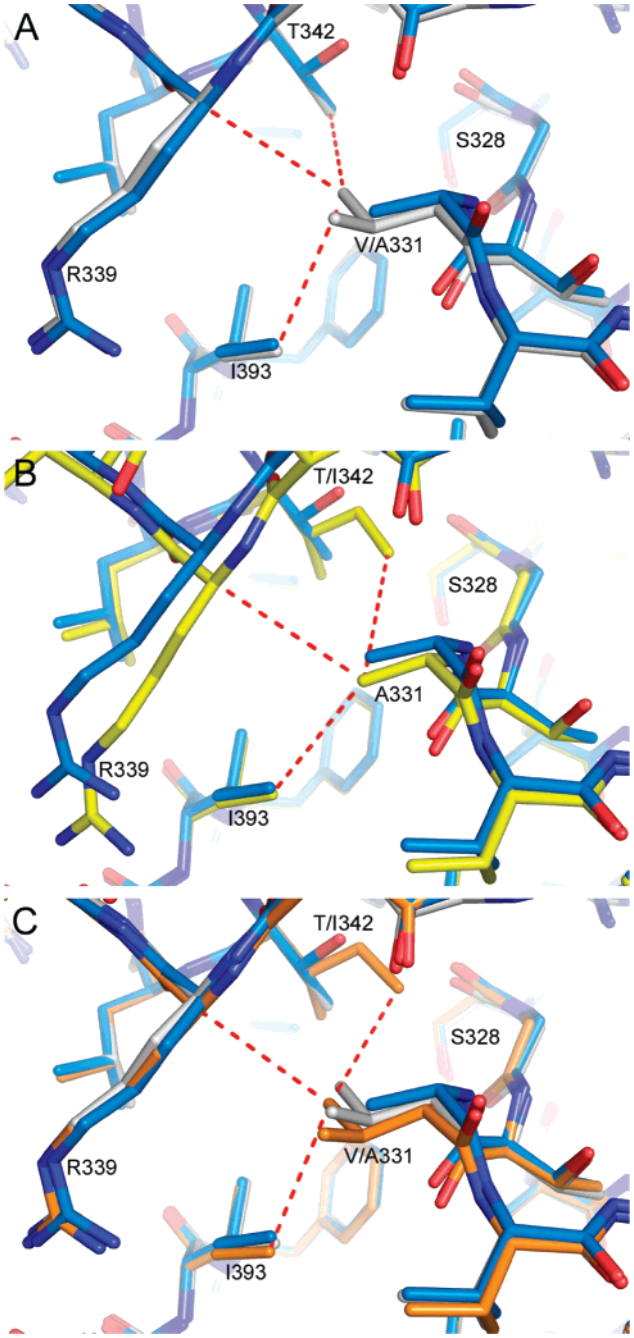

FIGURE 5: Interactions of residue 331. (A) Superposition of the wild-type (carbon atoms colored white) and V331A-mutant (carbon atoms colored blue) structures. The V331A substitution disrupts van der Waals interactions of residue 331 with Thr342, Arg339, and Ile393. (B) Superposition of the V331A-mutant (carbon atoms colored blue) and V331A/T342I-revertant (carbon atoms colored yellow) structures. The V331A/T342I-revertant substitutions cause a movement of main-chain atoms around large-subunit residue Arg339, restoring van der Waals interactions to Ala331. (C) Superposition of the supressor T342I (carbon atoms colored orange) with the wild-type (carbon atoms colored white) and V331A-mutant (carbon atoms colored blue) structures. The additional bulk of the Ile342 Cγ atom in T342I shifts the side chain of Val331 relative to that of the wild type and V331A.

T342I-suppressor enzyme causes a slight shift of the side chain of Val331 relative to that of the wild type and V331A (Figure 5C). Movement of the Arg339 backbone atoms was not observed in the T342I-suppressor enzyme due to the presence of the two Cβ atoms of Val331 (Figure 5C, Table 3). Thus, movement of Arg339 cannot be responsible for the similar kinetic properties of the V331A/T342I-revertant and T342I-suppressor enzymes (Table 1). However, whereas the Oγ atom of Thr342 makes a hydrogen bond to the carbonyl oxygen of Glu338 and a solvent-mediated hydrogen bond to the carbonyl oxygen of Ser328, these interactions are abolished when Thr342 is replaced by Ile in both the V331A/T342I-revertant and T342I-suppressor enzymes.

A shift of similar magnitude (0.96 Å) was observed for the Cα atom of Arg339 in the V331A/G344S-revertant enzyme (Table 3, Figure 4). In this case, the shift is a consequence of the displacement of almost the entire α-helix 6 (Figure 4). This displacement brings Thr342 significantly closer to Ala331 (Table 3, Figure 4). The substantial alterations resulting from the substitution of Gly344 with Ser may also be responsible for the altered catalytic properties of the G344S-suppressor enzyme (Table 1). However, the presence of Val331 may limit the displacement of α-helix 6, which may account for the different catalytic properties of the V331A/G344S-revertant and G344S-suppressor enzymes.

Alterations in the Active Site. Lys334 is located at the apex of loop 6 and interacts with substrate CO_2 in the CABP transition-state analogue (Figure 1) (*29*). Thus, Lys334 may be assumed to play a key role in the partitioning between carboxylation and oxygenation of the 2,3-enediolate of RuBP (*8*, *21*). However, despite the fact that CO_2/O_2 specificity is altered in all the mutant enzymes (*25*, *26*) (Table 1), the structural interaction between Lys334 and CABP is not disturbed (all shifts are within the coordinate error). Instead, there is a slight shift of the central part and the P2 phosphate group of bound CABP in the mutant enzymes. As a consequence, interactions between O3 of CABP and the Lys201 carbamate O1 is lengthened in the mutant enzymes (Table 4). More importantly, the V331A-mutant enzyme has significant increases in the hydrogen bond distances between CABP and the active-site residues Thr173 and Ser379 (Table 4). These distances are returned to near-wild-type values in the revertant and suppressor enzymes (Table 4). Such differences may contribute to the observed changes in kinetic constants.

Interactions with the Carboxy Terminus. As mentioned earlier, Glu338 interacts via a hydrogen bond between its carbonyl oxygen and Oγ of Thr342 in the wild-type and V331A-mutant enzymes. In the wild-type enzyme, the Glu338 side chain also makes solvent-mediated hydrogen bonds to main-chain atoms of Asp473 and Leu475 in the carboxy terminus of the large subunit (Figure 6). These interactions are either weakened or absent in the mutant enzymes. This is most pronounced in the D473E enzyme, where the carboxy terminus from residue 470 onward is disordered. However, Leu475 is also disordered in the V331A-mutant enzyme, and neither of the two solvent molecules is observed in the electron density maps. In the T342I-suppressor and V331A/T342I- and V331A/G344S-revertant enzymes, one water molecule is present, but the distance between the Glu338 amide nitrogen and the carbonyl oxygen of Asp473 is lengthened by 0.25, 0.55, and 0.80 Å, respectively.

The side chain of Asp473 may also be important in securing the carboxy terminus to the bulk of the large subunit (*16*, *28*). The carboxyl group of Asp473 makes ionic bonds with the guanidino nitrogen of Arg134 and the Nϵ of His310

Table 3: Contacts of Residue 331 (Å)[a]

atom pair	wild type	V331A	V331A/T342I	T342I	V331A/G344S
V331(Cγ2)−I393(Cδ1)	4.05			3.85	
V331(Cγ2)−T342(Cγ2)	3.95				
V331(Cγ2)−I342(Cδ1)				3.72	
V331(Cγ2)−R339(Cα)	4.09			3.80	
A331(Cβ)−I393(Cδ1)		4.28	4.05		4.17
A331(Cβ)−T342(Cγ2)		5.60			5.38
A331(Cβ)−T342(Oγ1)		5.06			4.46
A331(Cβ)−I342(Cδ1)			4.29		
A331(Cβ)−R339(Cα)		4.48	4.12		3.95

[a] Distances are mean distances in all subunits in the asymmetric unit.

Table 4: Distances between CABP and Several Active-Site Residues[a]

atom pair	wild type	V331A	V331A/T342I	T342I	V331A/G344S	D473E
CABP(O2)−T173(Oγ)	2.79	3.21	2.90	3.02	2.95	2.9
CABP(O3)−K201-carbamate(O1)	2.49	2.68	2.61	2.67	2.60	2.8
CABP(O4)−S379(O)	2.97	3.13	3.04	3.03	3.13	3.0
CABP(O4)−S379(Oγ)	2.90	3.19	2.72	3.11	3.08	2.9

[a] Distances are mean distances in all subunits in the asymmetric unit.

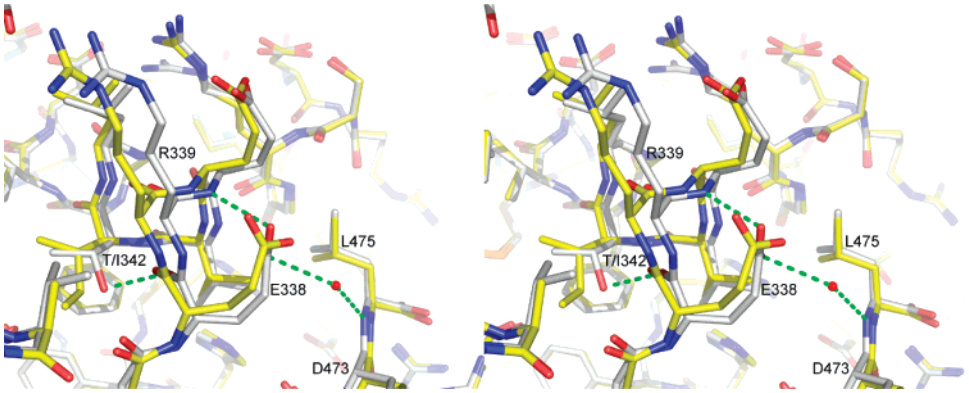

FIGURE 6: Stereo diagram showing interactions of Glu338 with residues in loop 6 and the carboxy terminus in the wild-type (carbon atoms colored white) and V331A/T342I-revertant (carbon atoms colored yellow) enzymes. The solvent molecule (red) is associated with the wild-type enzyme.

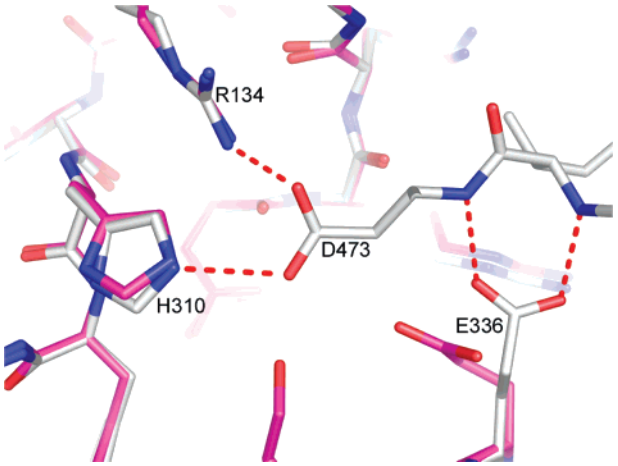

FIGURE 7: Interactions relative to Glu473 in the wild-type (white) and D473E-mutant (magenta) enzymes. Residue 473 is disordered in the D473E structure.

(Figure 7). In addition, the carboxy terminus is further secured by hydrogen bonding between the carboxyl of Glu336 and the backbone amides of Ile472 and Asp473. Because the carboxy terminus is disordered in the D473E-mutant enzyme, all these interactions are likely to be abolished, and the side chain of loop-6 Glu336 has an altered conformation (Figure 7). Despite these alterations, the D473E-mutant enzyme is able to bind CABP, and apart from the disordered carboxy-terminus, it displays all features of the closed state (i.e., ordering of loop 6 and the amino-terminal-domain loop of the adjacent large subunit).

Although the D473E substitution causes no gross perturbation of the structure of Rubisco apart from the disorder of the carboxy terminus, there are subtle alterations in the active site, including the conformation of CABP. This may contribute to the decreases in Ω, carboxylation catalytic efficiency, and tightness of CABP binding observed for the D473E and D473A mutant enzymes (*28*). However, because of the low-resolution limit (2.8 Å) of the D473E structure, it is not possible to quantify these changes.

DISCUSSION

The *Chlamydomonas rbcL*-V331A mutant and its photosynthesis-competent *rbcL*-V331A/T342I and *rbcL*-V331A/G344S revertants served as the first examples of genetic alterations that could both decrease and increase Rubisco CO_2/O_2 specificity (*25*, *26*). Because the mutant and suppressor residues flank active-site Lys334 in the flexible loop 6 (Figure 1), it was proposed that changes in the size of interacting side chains were responsible for disrupting/

restoring the hydrophobic core of loop 6, thereby influencing the interactions of the Lys334 side chain with the carboxylation and oxygenation transition states (*8*, *25*, *26*). A subsequent directed-mutagenesis study of *Synechococcus* Rubisco expressed in *E. coli* confirmed that the V331A substitution decreases Ω, but a T342I substitution alone did not alter the Ω value of otherwise wild-type Rubisco (*22*). Numerous directed-mutagenesis studies of loop 6 ensued (reviewed in refs *1* and *3*), but the molecular basis for the influence of loop 6 and its associated structural elements on Ω could not be rationalized beyond some alteration of loop-6 Lys334 (*1*, *8*, *21*). When the X-ray crystal structure was solved for the spinach enzyme, it was readily apparent that the V331A and T342I substitutions could, in fact, complement the bulk within the hydrophobic core of loop 6 (*19*). However, because Gly344 would not be directed toward the core of loop 6 (*19*), it was difficult to explain subsequently how the G344S-suppressor substitution would complement the low catalytic efficiency and specificity resulting from the original V331A-mutant substitution (*26*). X-ray crystal structures also revealed that the carboxy terminus could influence the loop-6 structure (*16*−*19*, *24*), and deletion of 10 carboxy-terminal residues from the Rubisco large subunit of *Synechococcus* caused a substantial decrease in Ω (*22*).

In the present study, with an objective to understand the role of loop 6 in catalytic efficiency and specificity, directed mutagenesis and chloroplast transformation of *Chlamydomonas* were employed to create the T342I and G344S loop-6 suppressor substitutions in the absence of the original V331A-mutant substitution. X-ray crystal structures were then solved for the *Chlamydomonas* mutant enzymes relevant to this region of the Rubisco structure.

As previously anticipated (*19*, *25*), the V331A substitution creates a cavity in the hydrophobic core of loop 6 that may be filled by solvent. In the V331A/T342I-revertant enzyme, the cavity is filled by the side chain of the T342I-suppressor substitution (Figure 3). The G344S suppressor substitution at least partly fills in the core of loop 6 due to displacement of α-helix 6 (Figure 4). However, despite a variety of alterations in the residues that comprise loop 6 and changes in the contacts between other residues and the CABP transition-state analogue, it is not readily apparent how changes in loop 6 may bring about changes in the interactions of residues with CABP. Contacts between CABP and the loop-6 active-site residue Lys334 are not significantly altered. Considering that a 60% decrease in Ω (for the V331A enzyme, Table 1) is equal to a change of only 2.3 kJ/mol in the difference of the free energies of activation for the carboxylation and oxygenation transition states (*8*), it may be difficult to see the exact structural basis for a change in Ω.

One plausible hypothesis to explain an effect of the V331A substitution on the active site concerns the backbone atoms of residues flanking Ala331. The main-chain atoms of Thr330 move slightly to compensate for the loss of bulk in loop 6. The Cγ2 atom of Thr330 is in van der Waals contact with the carbonyl oxygen of Ser379, and this distance may be shortened slightly. Together, these changes may be responsible for the significant lengthening of the hydrogen bond between Ser379 Oγ and CABP O4 (Table 4). Previous directed-mutagenesis studies with *R. rubrum*, *Synechococcus*, and *Chlamydomonas* Rubisco have shown that an S379A substitution greatly decreases the rate of carboxylation and alters Ω (*49*−*51*). Thus, it would seem reasonable to consider that an alteration affecting the interaction between Ser379 and CABP may be responsible for a decrease in Ω (Table 1).

The T342I-suppressor substitution restores the position of Thr330, but the V331A/T342I-revertant and T342I-suppressor enzymes have similar decreases in V_c and Ω, and increases in K_c and K_o, when compared with wild-type Rubisco (Table 1). This indicates that the T342I substitution affects the structure in the same way regardless of whether residue 331 is Val or Ala. In the V331A/T342I-revertant and T342I-suppressor enzyme structure, the Cδ1 atom of Ile342 forms a new van der Waals interaction with Gly329, which draws the Gly329 Cα away from CABP by 0.33 and 0.14 Å, respectively. This may influence the interactions of a number of residues with CABP in this region. In a previous directed-mutagenesis study of *Synechococcus* Rubisco, a G329A substitution eliminated carboxylase activity (*52*), further indicating that structural interactions focused on residues Ser379 and Gly329 may have a critical role in determining Ω.

Relative to the V331A-mutant enzyme, the V331A/G344S-revertant enzyme has an increase in Ω (Table 1), but the increased hydrogen-bond distance between CABP and the Ser379 carbonyl oxygen is similar in both enzymes (Table 4). Because the V331A/G344S-revertant and G344S-suppressor enzymes have different alterations in Rubisco catalytic properties (Table 1), it is likely that the G344S substitution alone produces changes in structure that cannot be deduced from only the V331A/G344S-revertant enzyme structure.

In the D473E crystal structure, the loss of hydrogen bonding between Glu336 and the backbone amides of Ile472 and Asp473 appears to cause a change in the interactions between CABP and Leu335. CABP O4P moves out of van der Waals contact with the Cβ and Cδ1 atoms of Leu335, with an increase in these distances of about 0.4 Å. Substitution of Leu335 with a variety of different residues also causes decreases in Ω (*53*, *54*).

In addition to the positional changes incurred by the mutant substitutions, it is also worth considering the effects of the substitutions on the flexibility and dynamics of the protein (*12*), effects that ultimately may be transmitted to the active site. The T342I substitution abolishes two hydrogen bonds of Oγ of the Thr342 side chain, one to the carbonyl oxygen of Glu338 and another to a solvent molecule. The loss of hydrogen bonding is likely to be destabilizing, but the magnitude of the effect also depends on the nature of the new amino acid side chain that is introduced. Substitutions that add or remove bulk (I342 and A331) are also likely to influence the dynamics of the loop.

The location of a Gly residue in the middle of an α-helix is relatively rare. Substitution of Gly344 in the middle of α-helix 6 of the α/β barrel is expected to add rigidity, but the Ser residue introduced in its place also has a relatively low α-helix propensity (*55*). Ser can participate in intrahelical hydrogen bonding, but may do so because it is the lowest energy option available. In the present structure, although the $i - 4$ main-chain carbonyl is present and available for hydrogen bonding, the Ser344 Oγ hydrogen bonds to the carbonyl O of Val341 at the $i - 3$ position, as well as to a local solvent molecule. This forces the side chain to adopt a

slightly strained conformation and hydrogen bonds of non-ideal geometry. Such strain may alter the dynamics of the adjacent loop, and the effects may ultimately be transmitted to the active site. Participation of the Ser hydroxyl in a hydrogen bond with a backbone carbonyl oxygen in the preceding turn of the α helix may also weaken the α-helical hydrogen bond in which the carbonyl oxygen is already participating.

The D473E substitution causes disorder of residues 470−475 of the carboxy terminus and disrupts a number of hydrogen bonds. Because these residues pack against α-helix 6 and loop 6 in the wild-type enzyme (Figure 1), the disorder is likely to influence loop-6 dynamics. These effects may be transmitted to the active site.

The X-ray crystal structures of mutant Rubisco enzymes illustrate the complexity of the structure, relatively distant from active-site residues, that must ultimately determine Rubisco catalytic efficiency and specificity. Although explanations for the influence of substituted residues on catalysis remain speculative, the ease of directed mutagenesis and chloroplast transformation in *Chlamydomonas*, coupled with genetic selection in vivo, may prove useful for further assessing the importance of the observed structural alterations.

ACKNOWLEDGMENT

We thank Dr. Todor Genkov for helpful discussions and Andreas Cederlund for excellent technical assistance. We are indebted to MAX-lab, Lund, Sweden, and ESRF and the EMBL Outstation, Grenoble, France, for providing beam time and data collection facilities.

REFERENCES

1. Spreitzer, R. J., and Salvucci, M. E. (2002) Rubisco: Structure, regulatory interactions, and possibilities for a better enzyme, *Annu. Rev. Plant Biol. 53*, 449−475.
2. Andersson, I., and Taylor, T. C. (2003) Structural framework for catalysis and regulation in ribulose-1,5-bisphosphate carboxylase/oxygenase, *Arch. Biochem. Biophys. 414*, 130−140.
3. Parry, M. A. J., Andralojc, R. A. C., Mitchell, P. J., Madgwick, P. J., and Keys, A. J. (2003) Manipulation of Rubisco: the amount, activity, function and regulation, *J. Exp. Bot. 54*, 1321−1333.
4. Spreitzer, R. J. (2003) Role of the Rubisco small subunit, *Arch. Biochem. Biophys. 414*, 141−149.
5. Houtz, R. L., and Portis, A. R. (2003) The life of ribulose 1,5-bisphosphate carboxylase/oxygenase—posttranslational facts and mysteries, *Arch. Biochem. Biophys. 414*, 150−158.
6. Andrews, T. J., and Whitney, S. M. (2003) Manipulating ribulose bisphosphate carboxylase/oxygenase in the chloroplasts of higher plants, *Arch. Biochem. Biophys. 414*, 159−169.
7. Laing, W. A., Ogren, W. L., and Hageman, R. H. (1974) Regulation of soybean net photosynthetic CO_2 fixation by the interaction of CO_2, O_2 and ribulose 1,5-diphosphate carboxylase, *Plant Physiol. 54*, 678−685.
8. Chen, Z., and Spreitzer, R. J. (1992) How various factors influence the CO_2/O_2 specificity of ribulose-1,5-bisphosphate carboxylase/oxygenase, *Photosynth. Res. 31*, 157−164.
9. Jordan, D. B., and Ogren, W. L. (1981) Species variation in the specificity of ribulosebisphosphate carboxylase/oxygenase, *Nature 291*, 513−515.
10. Read, B. A., and Tabita, F. R. (1994) High substrate specificity factor ribulose bisphosphate carboxylase/oxygenase from eukaryotic marine algae and properties of recombinant cyanobacterial Rubisco containing "algal" residue modifications, *Arch. Biochem. Biophys. 312*, 210−218.
11. Uemura, K., Anwaruzzaman, Miyachi, S., and Yokota, A. (1997) Ribulose-1,5-bisphosphate carboxylase/oxygenase from thermophilic red algae with a strong specificity for CO_2 fixation, *Biochem. Biophys. Res. Commun. 233*, 568−571.
12. Karkehabadi, S., Taylor, T. C., Spreitzer, R. J., and Andersson, I. (2005) Altered intersubunit interactions in crystal structures of catalytically-compromised ribulose-1,5-bisphosphate carboxylase/oxygenase, *Biochemistry 44*, 113−120.
13. Karkehabadi, S., Peddi, S. R., Anwaruzzaman, M., Taylor, T. C., Cederlund, A., Genkov, T., Andersson, I., and Spreitzer, R. J. (2005) Chimeric small subunits influence catalysis without causing global conformational changes in the crystal structure of ribulose-1,5-bisphosphate carboxylase/oxygenase, *Biochemistry 44*, 9851−9861.
14. Spreitzer, R. J., Peddi, S. R., and Satagopan, S. (2005) Phylogenetic engineering at an interface between large and small subunits imparts land-plant kinetic properties to algal Rubisco, *Proc. Natl. Acad. Sci. U.S.A. 102*, 17225−17230.
15. Andersson, I., Knight, S., Schneider, G., Lindqvist, Y., Lundqvist, T., Branden, C. I., and Lorimer, G. H. (1989) Crystal structure of the active site of ribulose-bisphosphate carboxylase, *Nature 337*, 229−234.
16. Duff, A. P., Andrews, T. J., and Curmi, P. M. G. (2000) The transition between the open and closed states of Rubisco is triggered by the inter-phosphate distance of the bound bisphosphate, *J. Mol. Biol. 298*, 903−916.
17. Schreuder, H. A., Knight, S., Curmi, P. M. G., Andersson, I., Cascio, D., Brändén, C.-I., and Eisenberg, D. (1993) Formation of the Rubisco active site by a disorder-order transition from the unactivated to the activated form, *Proc. Natl. Acad. Sci. U.S.A. 90*, 9968−9972.
18. Taylor, T. C., and Andersson, I. (1996) Structural transitions during activation and ligand binding in hexadecameric Rubisco inferred from the crystal structure of the activated unliganded spinach enzyme, *Nat. Struct. Biol. 3*, 95−101.
19. Knight, S., Andersson, I., and Brändén, C.-I. (1990) Crystallographic analysis of ribulose 1,5-bisphosphate carboxylase from spinach at 2.4 Å resolution: Subunit interactions and the active site, *J. Mol. Biol. 215*, 113−160.
20. Soper, T. S., Mural, R. J., Larimer, F. W., Lee, E. H., Machanoff, R., and Hartman, F. C. (1988) Essentiality of Lys-329 of ribulose-1,5-bisphosphate carboxylase/oxygenase from *Rhodospirillum rubrum* as demonstrated by site-directed mutagenesis, *Protein Eng. 2*, 39−44.
21. Lorimer, G. H., Chen, Y. R., and Hartman, F. C. (1993) A role for the epsilon-amino group of lysine-334 of ribulose-1,5-bisphosphate carboxylase in the addition of carbon-dioxide to the 2,3-enediol(ate) of ribulose 1,5-bisphosphate, *Biochemistry 32*, 9018−9024.
22. Gutteridge, S., Rhoades, D. F., and Herrmann, C. (1993) Site-specific mutations in a loop region of the C-terminal domain of the large subunit of ribulose bisphosphate carboxylase/oxygenase that influence substrate partitioning, *J. Biol. Chem. 268*, 7818−7824.
23. Harpel, M. R., and Hartman, F. C. (1994) Chemical rescue by exogenous amines of a site-directed mutant of ribulose-1,5-bisphosphate carboxylase/ oxygenase that lacks a key lysyl residue, *Biochemistry 33*, 5553−5561.
24. Newman, J., and Gutteridge, S. (1993) The X-ray structure of *Synechococcus* ribulose-bisphosphate carboxylase/oxygenase-activated quaternary complex at 2.2-Å resolution, *J. Biol. Chem. 268*, 25876−25886.
25. Chen, Z., and Spreitzer, R. J. (1989) Chloroplast intragenic suppression enhances the low specificity of mutant ribulose-1,5-bisphosphate carboxylase/oxygenase, *J. Biol. Chem. 264*, 3051−3053.
26. Chen, Z., Yu, W., Lee, J. H., Diao, R., and Spreitzer, R. J. (1991) Complementing amino-acid substitutions within loop-6 of the α/β-barrel active-site influence the CO_2/O_2 specificity of chloroplast ribulose-1,5-bisphosphate carboxylase/oxygenase, *Biochemistry 30*, 8846−8850.
27. Parry, M. A. J., Madgwick, P., Parmar, S., Cornelius, M. J., and Keys, A. J. (1992) Mutations in loop six of the large subunit of ribulose-1,5-bisphosphate carboxylase affect substrate specificity, *Planta 187*, 109−112.
28. Satagopan, S., and Spreitzer, R. J. (2004) Substitutions at the Asp-473 latch residue of *Chlamydomonas* ribulosebisphosphate carboxylase/ oxygenase cause decreases in carboxylation and CO_2/O_2 specificity, *J. Biol. Chem. 279*, 14240−14244.
29. Taylor, T. C., Backlund, A., Björhall, K., Spreitzer, R. J., and Anderson, I. (2001) First crystal structure of Rubisco from a green alga, *Chlamydomonas reinhardtii*, *J. Biol. Chem. 276*, 48159−48164.

30. Spreitzer, R. J., and Mets, L. (1981) Photosynthesis-deficient mutants of *Chlamydomonas reinhardtii* with associated light-sensitive phenotypes, *Plant Physiol. 67*, 565−569.
31. Goldschmidt-Clermont, M. (1991) Transgenic expression of aminoglycoside adenine transferase in the chloroplast: a selectable marker of site-directed transformation of *Chlamydomonas*, *Nucleic Acids Res. 19*, 4083−4089.
32. Du, Y. C., and Spreitzer, R. J. (2000) Suppressor mutations in the chloroplast-encoded large subunit improve the thermal stability of wild-type ribulose-1,5-bisphosphate carboxylase/oxygenase, *J. Biol. Chem. 275*, 19844−19847.
33. Braman, J., Papworth, C., and Greener, A. (1996) Site-directed mutagenesis using double-stranded plasmid DNA templates, *Methods Mol. Biol. 57*, 31−44.
34. Finer, J. J., Vain, P., Jones, M. W., and McMullen, M. D. (1992) Development of the particle inflow gun for DNA delivery to plant cells, *Plant Cell Rep. 11*, 323−328.
35. Spreitzer, R. J., and Chastain, C. J. (1987) Heteroplasmic suppression of an amber mutation in the *Chlamydomonas* chloroplast gene that encodes the large subunit of ribulosebisphosphate carboxylase/oxygenase, *Curr. Genet. 11*, 611−616.
36. Chen, Z., Chastain, C. J., Al-Abed, S. R., Chollet, R., and Spreitzer, R. J. (1988) Reduced CO_2/O_2 specificity of ribulose-1,5-bisphosphate carboxylase/oxygenase in a temperature-sensitive chloroplast mutant of *Chlamydomonas reinhardtii*, *Proc. Natl. Acad. Sci. U.S.A. 85*, 4696−4699.
37. Jordan, D. B., and Ogren, W. L. (1981) A sensitive assay procedure for simultaneous determination of ribulose-1,5-bisphosphate carboxylase and oxygenase activity, *Plant Physiol. 67*, 237−245.
38. Spreitzer, R. J., Jordan, D. B., and Ogren, W. L. (1982) Biochemical and genetic analysis of an RuBP carboxylase/oxygenase-deficient mutant and revertants of *Chlamydomonas reinhardtii*, *FEBS Lett. 148*, 117−121.
39. Kuehn, G. D., and Hsu, T. C. (1978) Preparative-scale enzymic synthesis of D-[^{14}C]ribulose 1,5-bisphosphate, *Biochem. J. 175*, 909−912.
40. Otwinowski, Z., and Minor, W. (1997) Processing of X-ray diffraction data collected in oscillation mode, *Methods Enzymol. 276*, 307−326.
41. Vagin, A., and Teplyakov, A. (1997) MOLREP: An automated program for molecular replacement, *J. Appl. Crystallogr. 30*, 1022−1025.
42. Collaborative Computational Project, Number 4 (1994) The CCP4 suite-programs for protein crystallography, *Acta Crystallogr. D50*, 760−763.
43. Murshudov, G. N., Vagin, A. A., and Dodson, E. J. (1997) Refinement of macromolecular structures by the maximum-likelihood method, *Acta Crystallogr. D53*, 240−255.
44. Perrakis, A., Sixma, T. K., Wilson, K. S., and Lamzin, V. S. (1997) wARP: Improvement and extension of crystallographic phases by weighted averaging of multiple-refined dummy atomic models, *Acta Crystallogr. D53*, 448−455.
45. Pannu, N. S., and Read, R. J. (1996) Improved structure refinement through maximum likelihood, *Acta Crystallogr. A52*, 659−668.
46. Jones, T. A., Zou, J.-Y., Cowan, S. W., and Kjeldgaard, M. (1991) Improved methods for building protein models in electron-density maps and the location of errors in these models, *Acta Crystallogr. A47*, 110−119.
47. Larson, E. M., O'Brien, C. M., Zhu, G., Spreitzer, R. J., and Portis, A. R. (1997) Specificity for activase is changed by a Pro-89 to Arg substitution in the large subunit of ribulose-1,5-bisphosphate carboxylase/oxygenase, *J. Biol. Chem. 272*, 17033−17037.
48. Ott, C. M., Smith, B. D., Portis, A. R., and Spreitzer, R. J. (2000) Activase region on chloroplast ribulose-1,5-bisphosphate carboxylase/ oxygenase: Nonconservative substitution in the large subunit alters species specificity of protein interaction, *J. Biol. Chem. 275*, 26241−26244.
49. Harpel, M. R., and Hartman, F. C. (1992) Enhanced CO_2/O_2 specificity of a site-directed mutant of ribulosebisphosphate carboxylase/oxygenase, *J. Biol. Chem. 267*, 6475−6478.
50. Lee, G. J., and McFadden, B. A. (1992) Serine-376 contributes to the binding of substrate by ribulose-bisphosphate carboxylase/oxygenase from *Anacystis nidulans*, *Biochemistry 31*, 2304−2308.
51. Zhu, G., and Spreitzer, R. J. (1994) Directed mutagenesis of chloroplast ribulose-bisphosphate carboxylase/oxygenase: substitutions at large subunit asparagine 123 and serine 379 decrease CO_2/O_2 specificity, *J. Biol. Chem. 269*, 3952−3956.
52. Cheng, Z. Q., and McFadden, B. A. (1998) A study of conserved in-loop and out-of-loop glycine residues in the large subunit of ribulose bisphosphate carboxylase/oxygenase by directed mutagenesis, *Protein Eng. 11*, 457−465.
53. Lee, G. J., McDonald, K. A., and McFadden, B. A. (1993) Leucine 332 influences the CO_2/O_2 specificity factor of ribulose-1,5-bisphosphate carboxylase/oxygenase from *Anacystis nidulans*, *Protein Sci. 2*, 1147−1154.
54. Whitney, S. M., von Caemmerer, S., Hudson, G. S., and Andrews, T. J. (1999) Directed mutation of the Rubisco large subunit of tobacco influences photorespiration and growth, *Plant Physiol. 121*, 579−588.
55. Blaber, M., Zhang, X. J., Lindstrom, J. D., Pepiot, S. D., Baase, W. A., and Matthews, B. W. (1994) Determination of α-helix propensity within the context of a folded protein, *J. Mol. Biol. 235*, 600−624.

BI701063F